RSC Advances

PAPER

View Article Online
View Journal | View Issue

Cite this: *RSC Adv.*, 2025, **15**, 7962

Quantifying how the *cis*/*trans* ratio of *N*,*N*-dimethyl-3,5-dimethylpiperidinium hydroxide impacts the growth kinetics, composition and local structure of SSZ-39†

Zheng Cui, [a] Charles E. Umhey,[b] Onyinyechukwu C. Ukagha,[a] Motunrayo Ogunleye, [a] Jean-Sabin McEwen *[bcdef] and Daniel F. Shantz *[a]

This work integrates experiments and computational methods to quantify how the *cis*/*trans* ratio of the OSDA used in SSZ-39 synthesis impacts the crystallization kinetics, material properties, and final product composition. The crystallization kinetics increase by 30% when increasing the *trans* isomer content from 14% to 80%. Per prior work, in all cases based on the synthesis gel composition and product yield aluminum is the limiting reagent, and the absence of any amorphous material detected in the time resolved PXRD studies leads us to conclude that FAU dissolution is the rate limiting step in the formation of SSZ-39 in this synthesis protocol. The TGA and NMR results suggest that the *trans* isomer of OSDA is selectively incorporated into the product. The NMR binding studies, and corresponding DFT-based results show that the *trans* isomer binds to FAU more strongly than the *cis* isomer, providing one possible explanation for this enhancement in kinetics and preferential uptake of the *trans* isomer. The EDS analysis indicates that the Si/Al ratios are between 7.7 and 8.6 at low and high *trans* OSDA content, indicating zeolite composition is mildly sensitive to the *trans* isomer content. EDS results show this decrease in aluminum content leads to a corresponding decrease in sodium uptake. DFT-based calculations confirm OSDA–sodium interactions cannot explain any decrease in sodium uptake, reinforcing lower aluminum content as the cause of lower sodium uptake. Preliminary cobalt titration experiments show a surprisingly low cobalt uptake but also show a clear dependence of the cobalt uptake on the solution pH.

Received 6th December 2024
Accepted 19th February 2025

DOI: 10.1039/d4ra08620a

rsc.li/rsc-advances

1 Introduction

The synthesis of zeolites is an active and vibrant field, with new materials being discovered regularly that will have implications for a range of current and emerging applications.[1] Small-pore zeolites, the focus of this work, have found extensive use in technologies ranging from NO_x abatement[2,3] to methanol to olefins,[4,5] and show potential in olefin/paraffin separations.[6] They are and will continue to be an active area of research.

How zeolites form is also an active research space. The most common way to make zeolites is *via* hydrothermal synthesis.[7–10] In this method, zeolites are synthesized in the presence of a silica source, aluminum source, the organic structure directing agent (OSDA) and alkali cations.[11,12] Starting with work by Zones in the 1990s, it was shown that one zeolite can be used as the aluminum source and participate in the process of being converted into a new zeolitic phase.[13] In recent years, interzeolite conversion has attracted interest in the zeolite synthesis community, and it has been proved to be an efficient way to prepare a range of small-pore zeolites including CHA, AEI, and AFX.[14–16]

Zeolite SSZ-39, an aluminosilicate with the so-called AEI topology that can be synthesized by interconversion from faujasite (FAU), has shown promise for the selective catalytic reduction of NO_x (SCR),[17,18] methanol to olefins,[19] and potentially methane-to-methanol.[20,21] Recently, Sano and co-workers did a systemic study of the interzeolite conversion from FAU to AEI in the presence of different organic structure directing

[a]*Department of Chemical and Biomolecular Engineering, Tulane University, 6823 St. Charles Avenue, New Orleans, LA 70118, USA. E-mail: dshantz@tulane.edu*
[b]*The Gene and Linda Voiland School of Chemical Engineering and Bioengineering, Washington State University, Pullman, WA 99164, USA*
[c]*Institute for Integrated Catalysis, Pacific Northwest National Laboratory, Richland, WA 99352, USA*
[d]*Department of Physics and Astronomy, Washington State University, Pullman, WA 99164, USA*
[e]*Department of Chemistry, Washington State University, Pullman, WA 99164, USA*
[f]*Department of Biological Systems Engineering, Washington State University, Pullman, WA 99164, USA*

† Electronic supplementary information (ESI) available. See DOI: https://doi.org/10.1039/d4ra08620a

agents (OSDAs) including *N*,*N*-dimethyl-3,5-dimethylpiperidinium hydroxides,[22] which is a mixture of *cis* and *trans* isomers obtained from SACHEM that we studied in this work. Prior work by Dusselier and coworkers showed that the identity of the isomer had an influence on synthesis, with the *trans* isomer being preferentially incorporated in the as-made zeolite.[23] Subsequent work from the Shantz Lab validated Dusselier and coworkers' findings and provided a more thorough study of how the *trans* isomer influenced crystallization kinetics, product composition, and how the aluminum was clearly the limiting reagent in synthesis.[12] Subsequent work from our lab showed that compositionally identical (Si/Al, Cu contents) samples of SSZ-39 made in the presence of differing amounts of the *trans* OSDA behaved differently in the selective catalytic reduction (SCR) of NO_x,[18] and most recently we have shown that Cu-SSZ-39 is more active than Cu-SSZ-13 of similar composition for the methane-to-methanol reaction.[20] In this investigation, we couple experimental efforts with molecular simulations to better understand how the presence of the *trans* isomer impacts crystallization kinetics and to develop a deeper understanding for the origin of this. In addition to characterizing the solid products as a function of synthesis time when one still has both FAU and AEI present using SEM, TGA, and other methods, binding studies of the *cis* and *trans* isomer on FAU are performed as well as molecular simulations to provide a more fundamental understanding of why the *trans* isomer accelerates crystallization.

2 Experimental section

2.1 Materials

Sodium silicate (PQ Brand N, 28.9 wt% SiO_2, 8.9 wt% Na_2O) was obtained from PQ Corporation. Faujasite (FAU) ($SiO_2 : Al_2O_3 = 5.2 : 1$) was obtained from Zeolyst. Sodium hydroxide pellets (ACS grade) and 3-(trimethylsilyl)propionic-2,2,3,3-d_4 acid, sodium salt (98 atom% D) were obtained from Sigma Aldrich. *N*,*N*-Dimethyl-3,5-dimethylpiperidinium hydroxide (20–35 wt%, with *trans* isomer content of 14–80%) was obtained from SACHEM. Cobalt(II) nitrate hexahydrate (99%), cobalt(II) acetate tetrahydrate (ACS, 98–102%) and deuterium oxide (99.8 atom% D) were purchased from Thermo Scientific Chemicals. All reagents were used as received.

2.2 SSZ-39 synthesis

Per prior work in our lab, SSZ-39 was synthesized using FAU ($SiO_2 : Al_2O_3 = 5.2 : 1$) as the aluminum source from a gel composition of $1SiO_2 : 0.0167Al_2O_3 : 0.57NaOH : 0.14R + OH^- : 28H_2O$ (Si/Al = 30). As an example, SSZ-39 made with 14% *trans* content of OSDA was synthesized as follows. First, 4.33 g of sodium silicate were weighed out and placed in a Teflon jar, followed by adding 0.5 mL of 1 M NaOH solution. Then, 2.5 mL of 20 wt% organic structure-directing agent (OSDA) solution (mixture of *trans* and *cis* isomers, 14% *trans* by NMR) was added to this solution. To this mixture, 6.2 mL of deionized water was added. Then, the magnetic stir bar was placed in the solution and 0.17 g FAU was added before mixing for 2 h at room temperature. The mixture was then transferred to two Teflon-lined autoclaves and heated at 140 °C with rotation at 60 rpm for the indicated time ranging from 4 to 72 h. All data shown in the results section for samples at various time points were generated from samples made using this approach. The samples were then cooled down for 2 h, followed by filtration, washing with DI water until the filtrate pH was approximately 7, and dried at 100 °C overnight. The OSDA used, *N*,*N*-dimethyl-3,5-dimethylpiperidinium hydroxide, has two isomers, the *cis* and *trans* isomers which are shown in Scheme 1.

2.3 OSDA adsorption studies

To carry out the OSDA adsorption studies, OSDA solutions of differing concentrations ranging from 50 mM to 250 mM were prepared using 35 wt%, 20% *trans* content OSDA obtained from SACHEM. The different concentrations of OSDA solutions were confirmed by NMR using TMSP as an internal chemical shift reference and quantitative standard (300 μL of a 10 mM TMSP solution). Spectra were acquired with a 20 s delay time and 128 scans. One gram of FAU was added to 10 mL of OSDA solution which was then stirred for 24 hours at room temperature. Centrifugation at 5000 rpm for 20 min was performed to separate the liquid from the solids. 300 μL of this solution was pipetted out and added to the same amount of 10 mM TMSP solution in the NMR tube, and NMR was performed the same way as before adsorption.

2.4 Cobalt titration studies

Cobalt titration was performed using the method described by Di Iorio *et al.*[24] First, NH_4-SSZ-39 was prepared *via* aqueous phase ion-exchange. 0.18 g of calcined sample was exchanged in 27 mL of 1.0 M NH_4NO_3 solution at room temperature for 24 h (150 mL per g solids), followed by washing with 300 mL DI water. The sample was then dried at 100 °C overnight and converted to H-SSZ-39 by calcination. The cobalt exchange was performed by adding 0.15 g of calcined sample to 22.5 mL of 0.25 M $Co(II)(NO_3)_2$ solution (150 mL per g sample). This solution was stirred at room temperature for 4 hours, then filtered and washed with 10 mL of deionized water four times and dried at 100 °C overnight after the first exchange.

The sample was calcined at 550 °C before being exchanged again with a 0.5 M $Co(II)(NO_3)_2$ solution (150 mL per g sample). The filtration and calcination were performed the same way as after the first exchange before EDS analysis. Selected samples were also analyzed by ICP by Galbraith.

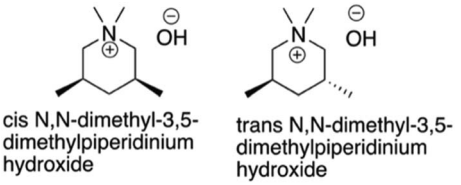

cis N,N-dimethyl-3,5-dimethylpiperidinium hydroxide

trans N,N-dimethyl-3,5-dimethylpiperidinium hydroxide

Scheme 1 Isomers of the OSDA used in this work.[12]

2.5 Analytical

Powder X-ray diffraction patterns were measured using a Rigaku Benchtop MiniFlex 600 X-ray diffractometer with Cu-Kα (l = 1.5418 Å) radiation operating at 40 kV and 15 mA. Materials were scanned in the range of $5° \leq 2\theta \leq 50°$ with a scanning speed of 1° min^{-1}. Field-emission scanning electron microscopy (FE-SEM) analyses were carried out using a Hitachi 4800 high-resolution scanning electron microscope operating at 3 kV. Energy-dispersive X-ray spectroscopy (EDS) was performed using a Hitachi S3400 system (30 V, 100 mA) for elemental analysis. Nitrogen adsorption measurements were performed using a Micromeritics ASAP 2020 system at 77 K. Approximately 0.05 g of calcined sample was degassed at 573 K for 18 h under high vacuum prior to each analysis. Micropore volumes were determined based on the volume of nitrogen adsorbed at a p/p_0 = 0.1, and external surface areas were calculated by the alpha-s method ($1.0 \leq \alpha_s \leq 1.5$). Thermal gravimetric analyses (TGA) were performed using a TA Instruments Q500 over a temperature range of 25–700 °C and a temperature ramping rate of 5 °C min^{-1} under flowing air. All ^{1}H NMR spectra were performed on a Bruker DRX 500 MHz NMR at room temperature. An inverse BBI probe was used. The resonance frequency of ^{1}H was 500.13 MHz and the pre-saturation pulse sequence for water suppression was used to acquire ^{1}H NMR spectra. ^{1}H NMR spectra of the filtrate recovered from the time series experiment were obtained from single pulse acquisition with a 30° pulse angle. Spectra were acquired with a 5 s delay time and 64 scans. For the ^{1}H NMR of the OSDA binding study, TMSP were used as an internal chemical shift reference as well as a quantitative standard (300 μL of a 10 mM solution). Spectra were acquired with a 20 s delay time and 128 scans were accumulated. For the analysis of the XRD shown, to estimate the relative amount of FAU and AEI, we use the integrated peak intensity of the FAU peak at 6.12° 2θ and the AEI peak 9.5° 2θ, *i.e.*, the fraction of AEI is equal to $I_{AEI,9.5}/(I_{AEI,9.5} + I_{FAU,6.12})$. In prior work, we used the peak heights instead of integrated intensities; we believe using the peak areas is more robust.

2.6 DFT calculations

All density functional theory calculations were performed using the Vienna *Ab initio* Simulation Package (VASP) version 6.[25–28] The interactions between valence and core electrons were modeled using the projector augmented wave method,[29] using PAW potentials released by VASP developers in 2017. The optB86b-vdW and optB88-vdW exchange–correlation functionals were used for all VASP calculations.[30,31] A 1 × 1 × 1 KPOINT mesh was used to sample the Brillouin zone with Gaussian smearing with a width of 0.2 eV. Self-consistent field cycles were considered converged once the total energy difference between steps was less than 1×10^{-5} eV. Geometries were considered converged when the norms of all forces were smaller than 0.02 eV Å^{-1}. Since spin polarized calculations converged to negligible magnetic moments, we preformed all calculations without spin polarization. The lattice parameters for our unit cell were identified by optimizing atomic coordinates while also allowing the cell shape to relax with a variety of different scaling factors and selecting the lattice parameters that minimized the final energy. These calculations identified an optimal cell volume of 3716.49 Å^3 (a = 17.39 Å, b = 17.41 Å, c = 17.38 Å, α = 60.02, β = 59.87, γ = 60.02) using the optB86b-vdW functional. A volume energy curve can be found in the ESI (Fig. S1†). The optimal unit cell using the optB88-vdW functional was also found to have a cell volume of 3716.49 Å^3 (a = 17.40, b = 17.39, c = 17.39, α = 59.98, β = 59.86, γ = 60.01).

3 Results

3.1 Confirmation of base synthesis

Initial work verified that SSZ-39 was reproducibly formed from the synthesis gel composition shown in the Experimental section. As expected, phase-pure SSZ-39 was formed from this mixture after heating for 72 hours at 140 °C based on indexing the powder diffraction pattern. The X-ray diffraction pattern and nitrogen adsorption isotherms for this material, and the parent FAU are included in the ESI (Fig. S2–S5†). Elemental analysis of the SSZ-39 and FAU by EDS shows the materials have Si/Al values of 7.71 ± 0.1 and 2.87 ± 0.09 respectively, where the standard deviations shown are calculated from nine separate measurements of the sample.

3.2 Interzeolite conversion rate investigation

We have previously shown that SSZ-39 growth kinetics were dependent on the *cis*/*trans* ratio of the OSDA,[12] consistent with prior work from Dusselier and coworkers.[23] Here, we investigate this with higher time resolution but also more thoroughly characterize the intermediate materials. Fig. 1 shows powder X-ray diffraction (PXRD) performed on the solids obtained as

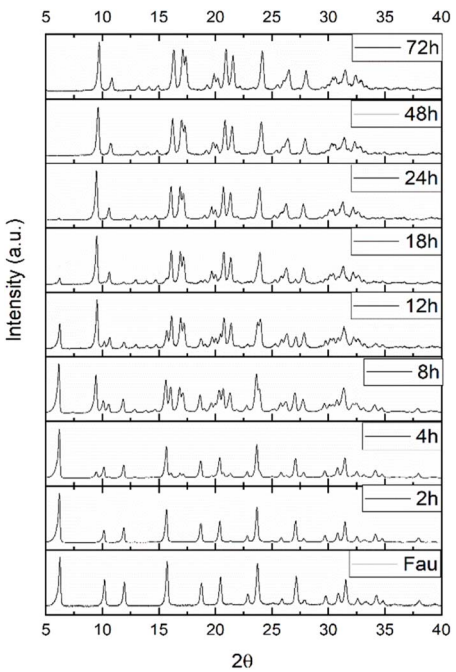

Fig. 1 PXRD results as a function of the heating time (14% *trans* content of OSDA).

a function of the synthesis time (14% *trans* isomer) to determine which phases are present (Fig. 1). Two phases were observed in all cases, faujasite (FAU) and SSZ-39 (AEI). Instead of full profile fitting to estimate the relative fractions of the two phases, the integrated intensities of the peak at 6.1° 2θ for FAU and 9.5° 2θ for SSZ-39 were compared. This method was validated using physical mixtures of known quantities of FAU and SSZ-39 for comparison (ESI Fig. S6†). Based on Fig. 1, SSZ-39 is first observed by PXRD at 4 hours of heating based on the appearance of the peak at 9.5° 2θ. Between 4 and 8 hours of heating the SSZ-39 peaks become more pronounced relative to the FAU peaks which is further observed with increasing time. This is most easily visualized by comparing the increased intensity of the SSZ-39 peak at 9.5° 2θ and the decreased intensity of the FAU at 6.1° 2θ.

After 24 hours of heating FAU is barely observable by PXRD (approximately 3% FAU present, Fig. 2). This indicates that based on PXRD, the conversion of FAU to SSZ-39 is complete in approximately 24 hours at a *trans* OSDA isomer content of 14%.

Finally, note that amorphous material is not observed at any of the time points, which would be manifested by a broad feature in the 2θ range of approximately 25°. This implies that the SSZ-39 forms at approximately the same rate as the FAU dissolves. The time-resolved PXRD data for the other samples is included in the ESI (Fig. S7–S11†).

Expanding upon this to look at the effect of the *cis*/*trans* ratio of OSDA used, Fig. 3 shows the mass fraction of SSZ-39 as a function of the heating time as well as the minimum time needed for complete consumption of FAU as determined by PXRD as a function of the OSDA *cis*/*trans* ratio (Fig. S7–S11†). Based on the results in Fig. 3, in the case of 14% *trans* content of OSDA, the synthesis appeared complete by PXRD after 30 hours, *i.e.* no FAU was detected by diffraction (integrated peak area for FAU at 6.1° 2θ is 0). In contrast, for the case of 80% *trans* content of OSDA, the sample is approximately 50% SSZ-39 at 8 h and the synthesis appears to be complete after 21 hours. The percent of solids yield is essentially constant across the four syntheses (23 to 24%), indicating the yield of SSZ-39 is insensitive to the *trans* content of OSDA used.

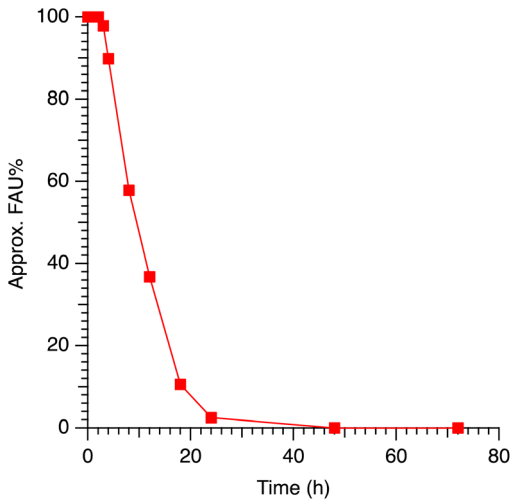

Fig. 2 Mass percent of FAU present as a function of reaction time estimated by powder X-ray diffraction for syntheses performed with a *trans* isomer content of 14%.

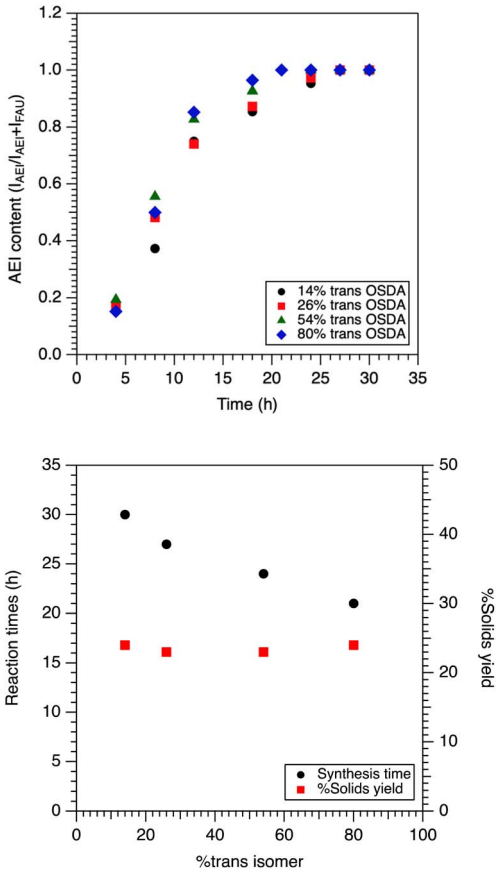

Fig. 3 (Top) relative amounts of SSZ-39 and FAU as a function of heating time for syntheses with four different *trans* isomer contents. (Bottom) minimum synthesis time for complete consumption of FAU and % solids yield for syntheses with four different *trans* isomer contents.

The figures above show syntheses with 80% *trans* content of OSDA resulted in an approximately 30% reduction in crystallization time when comparing to the reaction with 14% *trans* content of OSDA without a significant change in yield. The latter point is consistent with our prior work that indicated that nearly all the aluminum in the gel is incorporated in the final SSZ-39, and that by all appearances aluminum is the limiting reagent. Fig. 4 shows representative SEM images for the parent FAU used for SSZ-39 synthesis and the final SSZ-39 product. As can be seen, the FAU and SSZ-39 have different morphologies as well as particle sizes. The SSZ-39 zeolite possesses a uniform cuboid morphology and smaller size (300–350 nm) than the parent FAU. SEM images of the samples at all time points are included in the ESI (Fig. S12†).

Consistent with the PXRD results, the appearance of SSZ-39 crystals can be first seen at four hours of heating (Fig. 5). It appears that SSZ-39 particles are observed on the surface of the FAU particles. While it is tempting to speculate that the SSZ-39 grows directly off the surface (*i.e.* epitaxial growth of SSZ-39 off

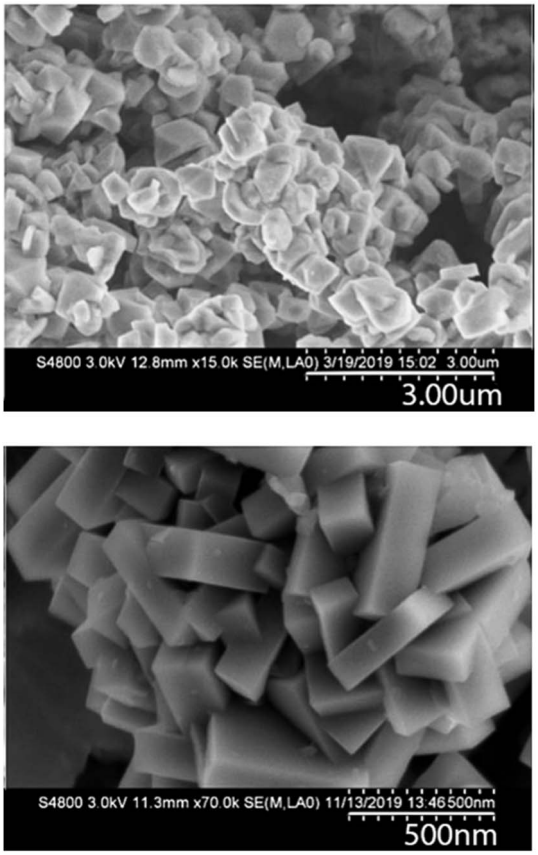

Fig. 4 SEM images of FAU (top) and SSZ-39 (bottom).

FAU), we do not have direct evidence for that. In contrast to the PXRD results where clear differences can be observed as the *cis*/*trans* ratio of the OSDA is varied, the time-resolved SEM at different *cis*/*trans* ratios is not as informative. One can see a more pronounced emergence of SSZ-39 crystals at shorter times (*i.e.*, 4–12 hours), beyond that there are no discernible differences in the SSZ-39 crystal shape/size as the *cis*/*trans* ratio is varied. Fig. 6 shows the derivative weight plots from TGA for the various syntheses as a function of time and *cis*/*trans* ratio. Two features stand out. First, there is a weight loss at approximately 300 °C that is observed at synthesis times before full crystallization, and then broadens and shifts to higher temperature as the synthesis finishes. We attribute this to the OSDA that is adsorbed on or in the FAU early in the synthesis. We attribute the shoulder left after the synthesis is completed to OSDA adsorbed on the outside of the SSZ-39. The derivative weight loss for FAU incubated with 100 mM OSDA for 24 h shown in the top left figure at the bottom supports this claim. There is a second feature that appears at approximately 430 °C, first noticeable at 8 h for 14% *trans*, which increases in intensity and shifts to approximately 10 degrees lower as the synthesis becomes complete.

This feature is assigned to the OSDA in the SSZ-39 cages. As can be seen in Fig. 6, the emergence of the high-temperature feature is more pronounced as the *cis*/*trans* ratio is increased, and the attenuation of the feature at 300 °C occurs at shorter synthesis times. The TGA results appear consistent with XRD and SEM that there are significant amounts of SSZ-39 formed by 8–12 hours in the syntheses.

Samples were also analyzed using nitrogen physisorption, with the objective of differentiating the two phases in the intermediate time points. This proved highly challenging, and ultimately uninformative. The first challenge that arose is that they have comparable micropore volumes, so comparing micropore volume evolution with time was inconclusive. We then performed measurements in the low-pressure region (defined here as $p/p_0 < 10^{-4}$), which also proved inconclusive.

3.3 Studies to quantify the selective uptake of *trans* isomer

This and prior work have shown that the *trans* isomer of the OSDA is selectively taken up during the SSZ-39 synthesis. Here we wish to try and better understand the why for this. To determine the *trans* content of the OSDA in the solid product is not trivial, and thus a two-step approach was taken. First, *via* TGA analysis, the total OSDA in the product was estimated from the weight loss in the temperature range of 200–600 °C. Subtracting this quantity from the initial amount of SDA used in the synthesis gives us an estimate of the amount of OSDA in

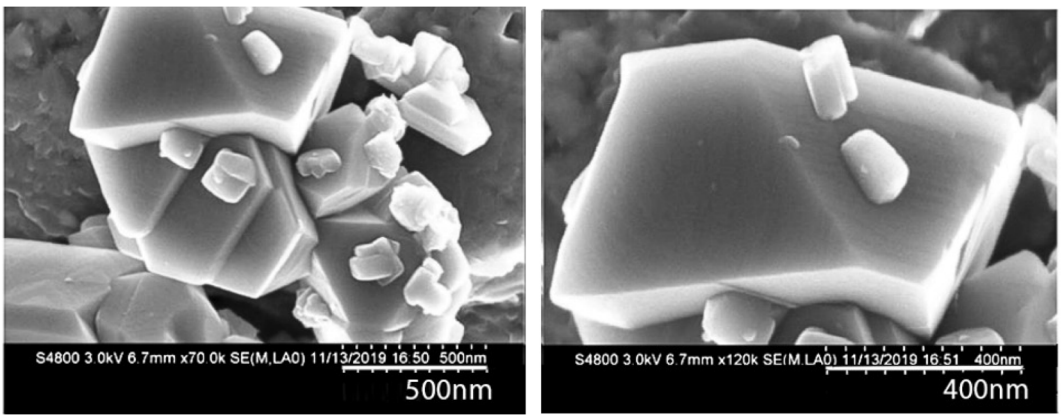

Fig. 5 SEM images of solids obtained after four hours of heating.

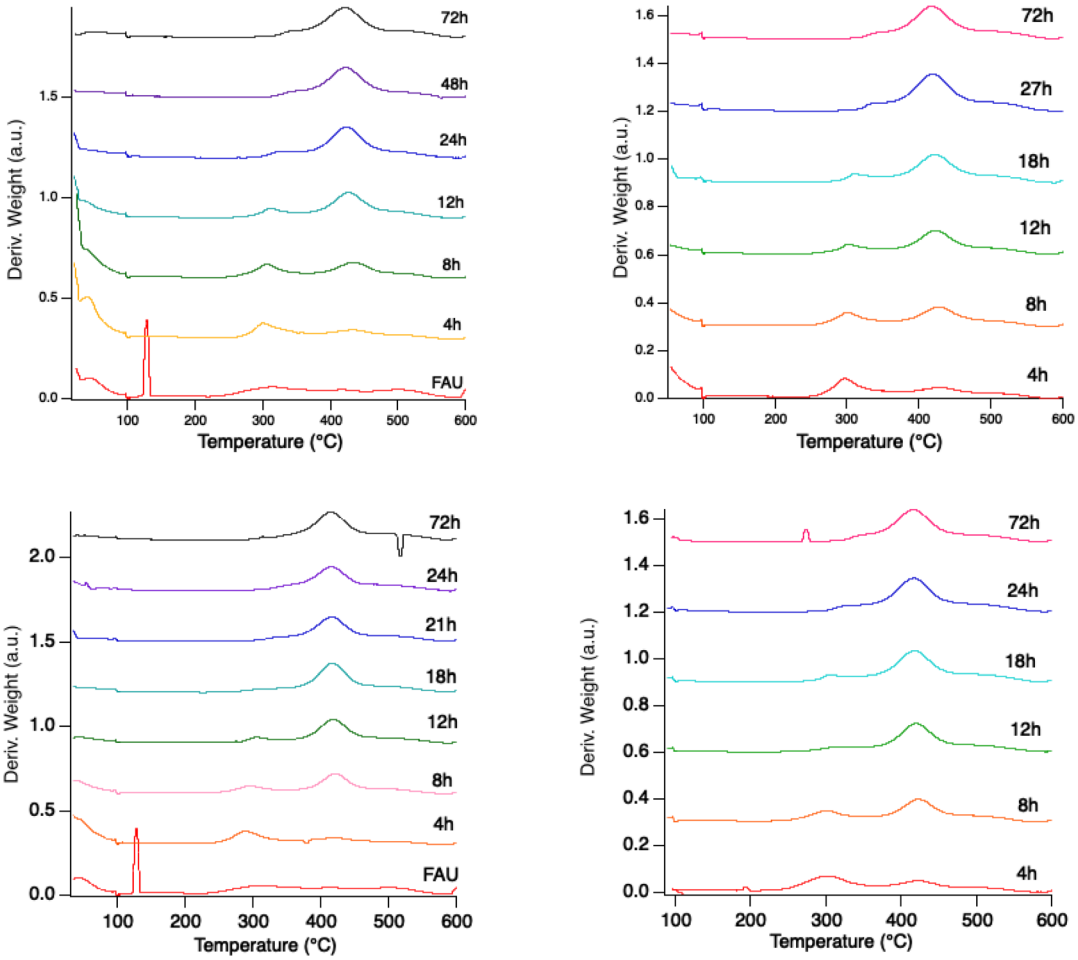

Fig. 6 (Clockwise from top left) differential weight loss plots as a function of synthesis times for samples made with 14%, 26%, 54%, and 80% *trans* OSDA.

solution after synthesis. The percentage of the *trans* isomer in the synthesis liquid after filtration was then determined by NMR.

This number was compared to the initial *trans* isomer content determined independently. A plot of this data is shown in Fig. 7, which shows that the *trans* isomer content in the liquid after synthesis is always lower than at the start of the synthesis, *i.e.*, the *trans* is selectively taken up. To probe this further, we chose to investigate if one isomer binds more strongly to the parent FAU particles than the other. The amount of bound OSDA (and its isomers) was estimated by performing NMR on the liquid obtained after 24 hours of incubating an OSDA solution with FAU. Fig. 8 (top) shows the amount of total OSDA bound as a function of solution concentration. Below a solution concentration of 50 mM where no appreciable signal is observed for the OSDA in the ^{1}H NMR, implying all (or nearly all) OSDA is adsorbed on the FAU. This limits our ability to measure the lower (<50 mM) solution concentration regime.

However, it is clear that the OSDA binds to or adsorbs into FAU in solution, given that at the solution concentration of 50 mM 97% of the total OSDA in solution is adsorbed. More interestingly, it is observed that the *trans* is preferentially adsorbed, given that the *cis*/*trans* ratio of the liquid obtained after incubation is higher, *i.e.*, depleted in *trans*, as compared to the initial ratio. The bottom of Fig. 8 shows a plot of the mole fraction of the *trans* isomer in solution before and after incubation with FAU. If the *cis* and *trans* isomer were adsorbed equally the points in red should all fall on the straight line, *i.e.*, $x_f = x_i$.

That they are below this line in all cases shows depletion of *trans* in solution with the initial mole fraction of 0.203 decreasing to anywhere in the range of 0.19 to 0.18. A possible explanation for this is provided in the Discussion (*vide infra*).

These results were supplemented by DFT calculations to determine the binding energy of both isomers to the FAU framework. Utilizing the optB86b-vdW functional, a binding energy of −357.75 kJ mol^{-1} for the *cis* isomer and −364.01 kJ mol^{-1} for the *trans* isomer, revealing a slight energetic preference for *trans* binding to FAU compared to *cis* binding. These results were replicated using the optB88-vdW functional where *cis* binding energies were calculated to be −358.93 kJ mol^{-1} and *trans* binding energies were calculated to be −365.52 kJ mol^{-1} revealing the same slight preference for *trans* adsorption. This preference for *trans* binding was

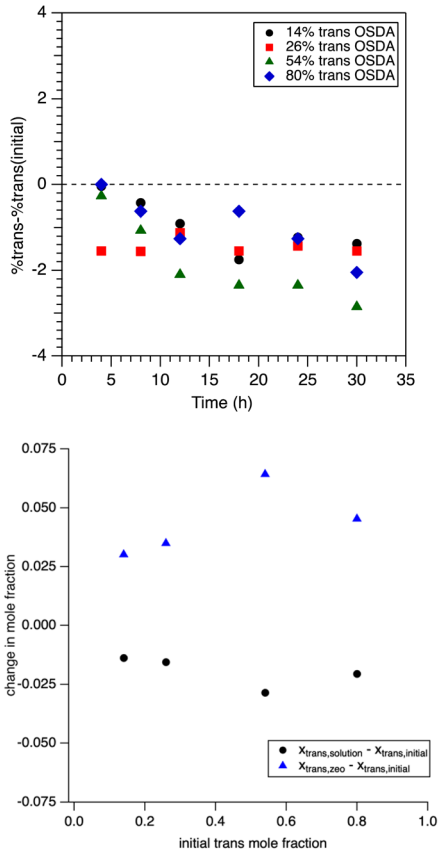

Fig. 7 (Top) change of the *trans* mole percent of OSDA in solution for various *trans* content of OSDA as a function of time. (Bottom) plot of the change in *trans* mole fraction for the OSDA in solution (black circle) and occluded in the final product after synthesis (blue diamond).

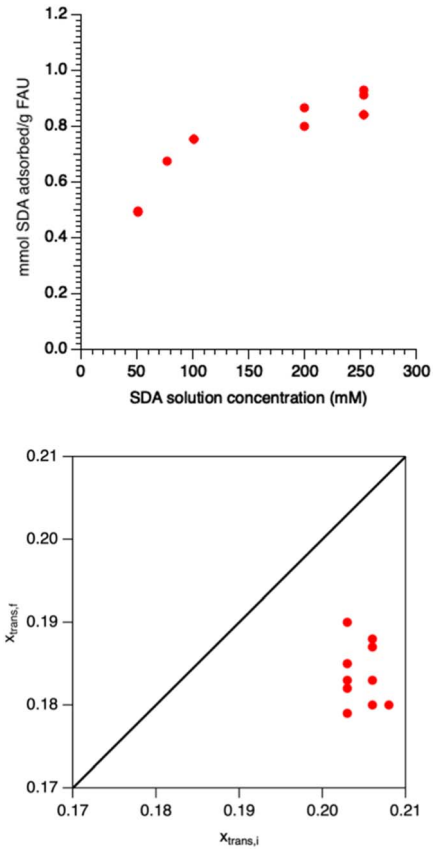

Fig. 8 (Top) binding isotherm of the OSDA to FAU, (bottom) plot of *trans* isomer mole fraction in solution before (*x*-axis) and after (*y*-axis) incubation with FAU.

maintained when *trans* binding was calculated in the presence of nearby sodium atoms (see Section 3.3). These results suggest the enhanced uptake of the *trans*-isomer during synthesis may be due to stronger binding between the FAU framework and the *trans* isomer, however since these calculations only examine OSDA–FAU, Na–FAU, and OSDA–Na interactions we cannot rule out OSDA–OSDA interactions decreasing the favorability of *trans* binding at high OSDA concentrations in the FAU framework. Steric constraints have been found to influence and even prohibit certain binding configurations in SSZ-39,[32] however FAU has a much larger cage size which likely reduces the impact of steric constraints. Additionally, OSDA–OSDA interactions are less likely to occur in dilute solutions like the solutions used in the NMR study discussed earlier. When the binding energies were calculated for the *cis* and *trans* OSDAs in SSZ-39 they were found to be significantly stronger than the binding energies in FAU for both *cis* and *trans* OSDAs (see Fig. 9), however no significant difference was observed between the binding energies of the *trans* OSDAs and *cis* OSDAs in SSZ-39.

3.4 Compositional properties

The work above, consistent with prior work, shows that increasing the *trans* isomer content enhances the crystallization kinetics of SSZ-39. Consistent with prior work, we also observe that increasing the *trans* isomer content in the synthesis gel has a small, but discernible effect of increasing the Si/Al ratio, as can be seen in Fig. 10. The yield of solids is essentially constant (within the sensitivity of the product work up/recovery after synthesis), consistent with the aluminum being the limiting reagent. The solids obtained directly from synthesis were also analyzed compositionally. Given the mixture of phases the

OSDA Isomer	FAU Configuration	SSZ-39 Configuration	FAU Binding Energy (kJ/mol)	SSZ-39 Binding Energy (kJ/mol)
Cis	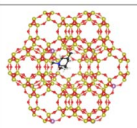	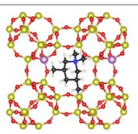	-357.75	-460.27
Trans	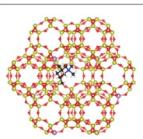	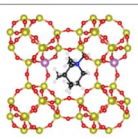	-364.01	-462.08

Fig. 9 Final configurations for *cis* and *trans* OSDA molecules adsorbed in FAU and the binding energies for the *cis* and the *trans* OSDA isomers. The red, yellow, cyan, black, blue and white spheres are O, Si, Al, C, N and H atoms, respectively.

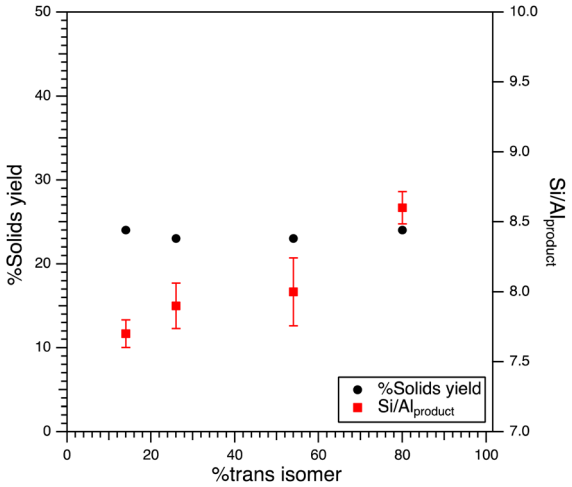

Fig. 10 Solids yields and Si/Al ratio for the fully crystallized product as a function of *trans* content of OSDA.

interpretation of that data is not trivial. The key observation is that, as expected, we see a systematic increase in the Si/Al of the solids obtained as the FAU is converted to SSZ-39 (Table S8†).

An item we have not reported on previously[23] is the presence of sodium in the as-made zeolite. EDS indicates that the samples do contain sodium, and the sodium content decreases as the Si/Al of the product obtained increases (Fig. 11). This makes sense, given that the weight percent of OSDA in the as-made zeolite is effectively constant, consistent with approximately one OSDA per cage.

To illustrate, in the case of a Si/Al = 8, there will be an average of 5.33 aluminum atoms per unit cell and there are four cages (and hence at most four OSDAs) per unit cell. This necessitates the presence on average of 1.33 sodium cations per unit cell for the material to satisfy charge neutrality. As can be seen in Fig. 11, the Na/Al ratio is approximately 0.4, which is

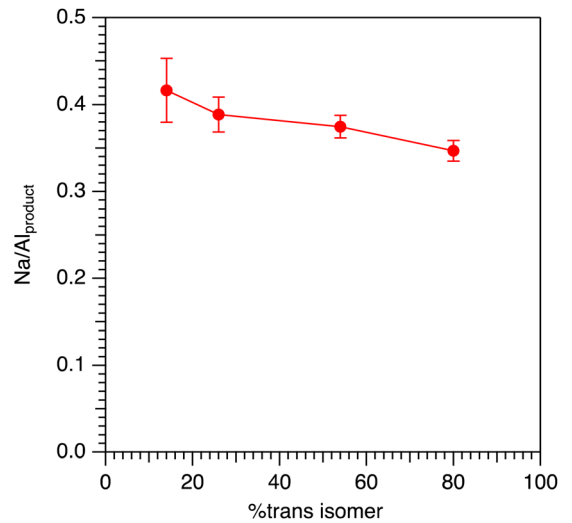

Fig. 11 Na/Al molar ratio of the product as a function of *trans* content of OSDA.

consistent with the logic above, and one can also see a small decline in the Na/Al ratio as one goes to samples made with higher *trans* content of OSDA (which have slightly higher Si/Al ratios). The results show that the presence of an increased *trans* isomer enables the formation of SSZ-39 with a slightly higher Si/Al ratio, with a concomitant reduction in the need for extra-framework sodium. DFT calculations using the optB86b-vdW functional were performed to systematically test the adsorption energies of sodium in SSZ-39 and FAU in the presence of *cis* and *trans* OSDAs. The details of these calculations are discussed in the ESI.† These calculations reveal that the isomer of coadsorbed OSDA molecules does not create any meaningful difference between sodium adsorption energies in FAU with binding energies differing by only 1.9 kJ mol^{-1}, which is within the error of our DFT calculations. Interestingly the presence of OSDA molecules did slightly enhance the binding energy of sodium in FAU making sodium binding 11.6–13.5 kJ mol^{-1} more favorable compared to the binding energy of sodium in the absence of OSDAs. Similarly, the presence of sodium slightly enhances the favorability of OSDA binding to the FAU framework making binding energies more favorable by 11.6 kJ mol^{-1} in the case of *cis* isomers and 17.4 kJ mol^{-1} in the case of *trans* isomers. While it is unclear if these results are due to interactions between the OSDA and sodium or interactions between either the OSDAs and sodium and the Al pair in the FAU framework, it is clear that the coadsorption of sodium and OSDA molecules is favorable. These computational results and the experimental results shown in Fig. 11 suggests that the decrease in sodium concentration in the zeolites is due to an increase in the Si : Al ratio caused by the *trans* OSDAs which creates fewer sites capable of hosting sodium making it more difficult for sodium atoms to adsorb to the zeolite rather than any OSDA–sodium interactions making sodium binding less favorable.

In SSZ-39, the DFT-based binding energy of sodium becomes less favorable (ranging from an increase of +11.0 kJ mol^{-1} to +11.4 kJ mol^{-1}) when sodium is adsorbed in SSZ-39 using a 50 : 50 mixture of *cis* and *trans* isomers to charge-compensate the aluminum. This difference is observed when compared to using either a pure *cis* or pure *trans* OSDA mixture, where sodium binding energies of −315.9 kJ mol^{-1} and −315.5 kJ mol^{-1} are obtained, respectively. Increasing the *trans* ratio from 50% to 100% did not continue the trend of making sodium binding less energetically favorable when compared to the pure *cis* case.

The less favorable binding energy with a 50 : 50 *cis–trans* mixture is likely due to this mixture favoring aluminum distributions that are less suitable for sodium binding, rather than any specific interactions between sodium and the *trans* isomer. If sodium-*trans* interactions were more repulsive than sodium-*cis* interactions, we would expect the binding energy to become even less favorable with higher *trans* content.

This hypothesis is supported by the fact that in SSZ-39 with three aluminum atoms, two aluminum atoms must occupy the same double six-membered ring (D6MR), forming a 2Al-D6MR subunit, while the third aluminum atom must occupy a separate D6MR (see Table S1†). When sodium is used to charge-compensate at the most favorable adsorption sites, the

sodium cations are within a 6 MR that is part of the 2Al-D6MR subunit.

With a pure *cis* and pure *trans* OSDA mixture, the ideal aluminum pair distribution places the aluminum atoms in separate D6MRs. This allows sodium to sit in the preferred double six-membered ring structure containing two aluminum atoms without forcing the OSDA molecules to shift from their ideal orientations (see Table S1†). In the pure *cis* OSDA mixture, the aluminum distribution is different compared to the pure *trans* case, both before and after adding the third aluminum atom to charge-compensate sodium. Despite these differences, the sodium atom remains in a 2Al-D6MR subunit in both cases, resulting in similar binding energies for sodium – −315.9 kJ mol^{-1} for pure *cis* and −315.5 kJ mol^{-1} for pure *trans*.

The aluminum distribution favored by a 50 : 50 *cis–trans* OSDA mixture is one where the aluminum atoms occupy the same D6MR, forcing the sodium atom to sit in a less favorable position, with only one aluminum atom in its D6MR. This position places the sodium atom in a D6MR where it interacts weakly with a single aluminum atom, since both aluminum atoms occupying the same D6MR are already charge-compensated by OSDA molecules. This configuration results in a sodium binding energy of −292.7 kJ mol^{-1} (see Table S2†).

Shifting the sodium atom to the more favorable D6MR containing two aluminum atoms improves the binding energy to −304.5 kJ mol^{-1}. However, for this shift to occur, one of the OSDA molecules must reorient to charge-compensate the aluminum atom that was previously compensated by sodium. Interestingly, when the energy penalty for this reorientation is calculated (see ESI Section SC 2.3†), it is found to be only 2.15 kJ mol^{-1}, which is within the margin of error for DFT calculations. This suggests that the rotation is not the cause of the lower binding energy observed in mixtures of *cis* and *trans* OSDAs.

Thus, this analysis indicates that the key source of the difference in sodium binding energy is likely due to the 50 : 50 *cis–trans* mixtures favoring aluminum distributions that are less favorable for sodium binding. While these results suggest that the aluminum distribution impacts sodium binding energies, the fact that sodium uptake decreases even when the *trans* content exceeds 50% means that one of the following possibilities is true: (i) the aluminum distribution in SSZ-39 is more complex than the idealized OSDA–zeolite interactions considered here, (ii) sodium binding in SSZ-39 cannot be fully explained by thermodynamic factors alone, or (iii) the previously hypothesized explanation is correct—that sodium uptake decreases due to *trans* OSDAs increasing the Si : Al ratio, which creates fewer sites capable of hosting sodium.

3.5 Cobalt titrations

To experimentally attempt to probe the issue of aluminum ordering, cobalt titrations were performed on several samples. Given that SSZ-39 and SSZ-13 are structurally similar as well as compositionally similar, studying this subject in SSZ-39 to compare to SSZ-13 seemed a worthy question to explore. This is further motivated by work in our lab showing that Cu-SSZ-39 and Cu-SSZ-13 of very similar compositions exhibit differing activity levels for both the partial oxidation of methane to methanol,[20] as well as the selective catalytic reduction of NO.[18]

Differing spatial distributions of aluminum in the lattice could be one contributing factor to this. The protocol of Di Iorio and co-workers was used to study SSZ-39.[24] Fig. 12 shows a plot of the Co/Al ratio of the samples investigated above.

This data is also replotted in the bottom of Fig. 12 where the Si/Al of the sample instead of the *trans* content in the gel is plotted on the *x*-axis to have a comparison with the findings of SSZ-13 in Di Iorio and coworkers' report, which shows SSZ-13 with a Si/Al = 5 has a Co/Al ratio of 0.19, and the SSZ-13 sample with a Si/Al = 15 has a Co/Al = 0.08.[24] As can be seen, the Co/Al ratios of our samples are much lower than what Di Iorio and coworkers report for SSZ-13 (ref. 24) and there is no obvious change in the fraction of Al pairs based on cobalt titration for different Si/Al of the material based on the Si/Al of

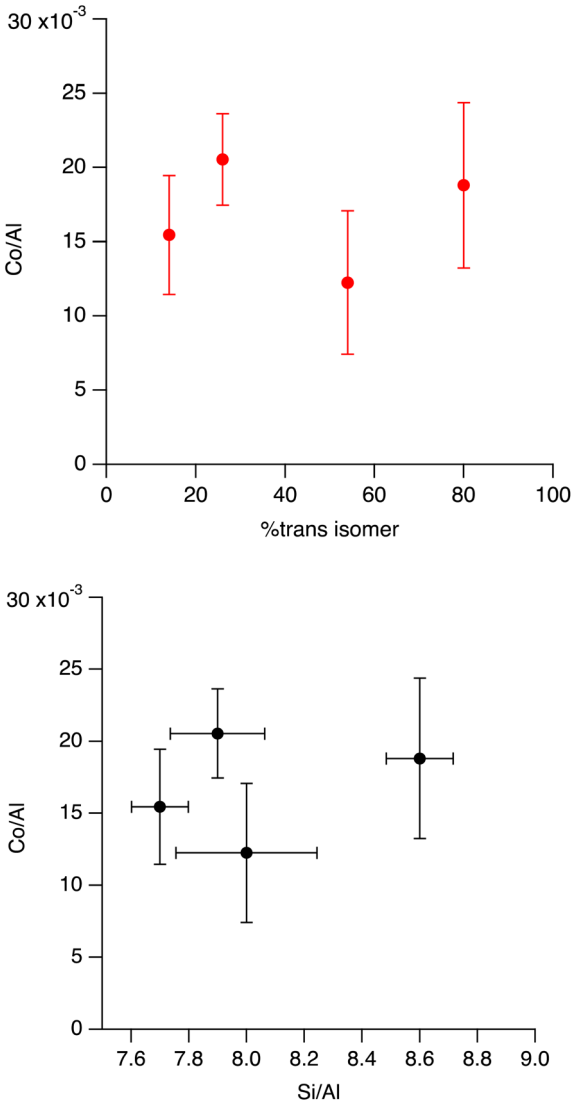

Fig. 12 (Top) Co/Al ratio for samples made with varying contents of *trans* isomer in the synthesis mixture. (Bottom) plot of samples Co/Al *versus* Si/Al for same samples.

our SSZ-39 samples with different *trans* content in the range of 7.7 to 8.6, and the parent FAU we used for the synthesis has a Co/Al = 0.1 ± 0.005. These results are somewhat surprising, as they would suggest there are very few aluminum pairs in these samples.

To probe this further, we decided to explore the cobalt uptake using the same process where the pH of the solution is modestly varied (pH varied between approximately 2 and 4), and also one where a different cobalt reagent was used (cobalt acetate) which results in a much higher initial pH. These results are shown in Fig. 13. As can be seen, the Co/Al ratio clearly correlates with the initial solution pH.

A few points are in order. First, the sample in Fig. 13 in the 'standard exchange' (pH ~ 3), has a lower cobalt uptake than the one shown in Fig. 12. Second, it is worth noting that the EDS values and their standard errors map well with the ICP results (single experimental point). This result points to the fact the pH of the solution plays an important, and to date not recognized, role in the ability to exchange cobalt into these materials. This is being explored further and will be reported elsewhere.

4 Discussion

The goal of this work was to try and better understand why syntheses with increased *trans* isomer in the synthesis gel led to accelerated synthesis rates. An expansion of our prior work characterizing the synthesis products as a function of heating time and gel *cis*/*trans* ratio is consistent with prior work. Namely, as the gel has more *trans* isomer the crystallization kinetics increase and the product Si/Al increase modestly.

We have not fully developed an answer to the 'why' for this. However, this work does clearly show that in the solution phase, the *trans* isomer binds/adsorbs more strongly on the FAU than the *cis* isomer. Calculations shown are consistent with this experimental result. It is also shown *via* FE-SEM, that the AEI crystals observed during the intermediate time periods where both phases are present always appear to be growing off the FAU surface. We do not have direct evidence for epitaxial growth. However, if the AEI crystals form at the FAU/water interface or near it, given there is enhancement of the *trans* isomer in the vicinity as shown by NMR this would explain why the *trans* isomer is enhanced in the final product. It does not, however, explain why the kinetics are accelerated. The only speculation we could posit here is when there is more *trans* isomer in the synthesis gel there are more OSDAs near/in the FAU and hence this drives the growth of AEI. But this is only speculation.

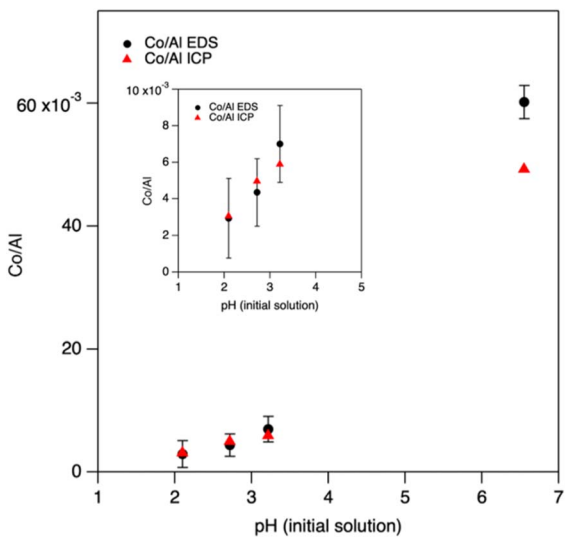

Fig. 13 (Top) Co/Al ratio of a SSZ-39 material made with 20% *trans* isomer as a function of the initial pH of the cobalt nitrate exchange solution. (Inset) magnification of the plot over pH range of one to five.

5 Conclusions

SSZ-39 was successfully synthesized by using different *trans* contents of OSDAs and characterized by using PXRD, SEM, EDS, TGA and N_2 adsorption at different time points of the inter-conversion of FAU to SSZ-39. Increasing the *trans* content of the OSDA for synthesis accelerated the zeolite crystallization with shorter reaction time to obtain pure phase SSZ-39, confirming the prior literature. The *trans* isomer of OSDA is taken up selectively into the product as suggested by TGA and NMR results. Based on our liquid-phase adsorption study, the *trans* isomer binds more strongly with FAU than the *cis* isomer. These results are supported by DFT-based calculations showing higher binding energies for *trans* isomers to FAU than *cis* isomer to FAU. EDS analysis of these samples showed Si/Al ratio from 7.7 to 8.6, indicating more than one Al atom per double six ring. These studies on synthesis of SSZ-39 over a wide range of *cis*/*trans* ratios of OSDA not only provide insights about how to potentially tailor active site arrangements in SSZ-39, but also give an interesting comparison to SSZ-13 materials, which our lab has shown previously display differing catalytic properties.[20,33,34]

Data availability

The data supporting this article can be found in the ESI.†

Conflicts of interest

This manuscript is submitted without any conflicts of interest and has been published with the consent of all authors.

Acknowledgements

The authors acknowledge NSF grant CBET-2035302 and CBET-2035280 for support. C. U. also acknowledges partial funding from the CeRCaS NSF IUCRC under grant number CBET-1939876. The authors thank Dr Jeewan Pokhrel for the SEM images. This work was partially funded by the Joint Center for Deployment and Research in Earth Abundant Materials (JCDREAM) in Washington State. This work also used Bridges-2 at the Pittsburgh Supercomputer Center through allocation CHE170068 from the Advanced Cyberinfrastructure Coordination Ecosystem: Services & Support (ACCESS) program,[35] which

is supported by National Science Foundation grants #2138259, #2138286, #2138307, #2137603, and #2138296. Additional computational resources were provided by the Kamiak HPC under the Center for Institutional Research Computing at Washington State University. We also thank the Kulkarni group for fruitful discussions. The Pacific Northwest National Laboratory is operated by Battelle for the U.S. DOE.

References

1 H. Xu and P. Wu, *Natl. Sci. Rev.*, 2022, **9**, nwac045.
2 J. Zhang, Z. Li, H. Yi, X. Tang, H. Cheng and Q. Yu, *Fuel*, 2023, **348**, 128577.
3 Q. Yu, H. Cheng, X. Tang, H. Yi, X. Ren and Z. Li, *J. Cleaner Prod.*, 2022, 135119.
4 Y. Zhou, J. Zhang, W. Ma, X. Yin, G. Chen, Y. Liu and J. Li, *Inorg. Chem. Front.*, 2022, **9**, 1752–1760.
5 J. Hua, X. Dong, J. Wang, C. Chen, Z. Shi, Z. Liu and Y. Han, *ACS Catal.*, 2020, **10**, 3009–3017.
6 D. Saha, M.-B. Kim, A. J. Robinson, R. Babarao and P. K. Thallapally, *Iscience*, 2021, **24**, 103042.
7 X. Meng and F.-S. Xiao, *Chem. Rev.*, 2014, **114**, 1521–1543.
8 T. Abdullahi, Z. Harun and M. H. D. Othman, *Adv. Powder Technol.*, 2017, **28**, 1827–1840.
9 C. S. Cundy and P. A. Cox, *Microporous Mesoporous Mater.*, 2005, **82**, 1–78.
10 C. S. Cundy and P. A. Cox, *Chem. Rev.*, 2003, **103**, 663–702.
11 H. Imai, N. Hayashida, T. Yokoi and T. Tatsumi, *Microporous Mesoporous Mater.*, 2014, **196**, 341–348.
12 R. Ransom, J. Coote, R. Moulton, F. Gao and D. F. Shantz, *Ind. Eng. Chem. Res.*, 2017, **56**, 4350–4356.
13 S. I. Zones, *J. Chem. Soc., Faraday Trans.*, 1990, **86**, 3467–3472.
14 C.-R. Boruntea, *Design, synthesis and characterization of small-pore zeolites for industrial environmental applications*, Universitat Politècnica de València, 2020.
15 T. Sonoda, T. Maruo, Y. Yamasaki, N. Tsunoji, Y. Takamitsu, M. Sadakane and T. Sano, *J. Mater. Chem. A*, 2015, **3**, 857–865.
16 R. Nedyalkova, C. Montreuil, C. Lambert and L. Olsson, *Top. Catal.*, 2013, **56**, 550–557.
17 H. Xu, L. Zhu, Q. Wu, X. Meng and F.-S. Xiao, *Inorg. Chem. Front.*, 2022, **9**, 1047–1057.
18 R. Ransom, R. Moulton and D. F. Shantz, *J. Catal.*, 2020, **382**, 339–346.
19 N. Martín, Z. Li, J. Martínez-Triguero, J. Yu, M. Moliner and A. Corma, *Chem. Commun.*, 2016, **52**, 6072–6075.
20 J. Pokhrel and D. F. Shantz, *J. Catal.*, 2023, **421**, 300–308.
21 A. Koishybay and D. F. Shantz, *J. Am. Chem. Soc.*, 2020, **142**, 11962–11966.
22 N. Tsunoji, D. Shimono, K. Tsuchiya, M. Sadakane and T. Sano, *Chem. Mater.*, 2020, **32**, 60–74.
23 M. Dusselier, J. E. Schmidt, R. Moulton, B. Haymore, M. Hellums and M. E. Davis, *Chem. Mater.*, 2015, **27**, 2695–2702.
24 J. R. Di Iorio and R. Gounder, *Chem. Mater.*, 2016, **28**, 2236–2247.
25 G. Kresse and J. Furthmüller, *Phys. Rev. B: Condens. Matter Mater. Phys.*, 1996, **54**, 11169–11186.
26 G. Kresse and J. Furthmüller, *Comput. Mater. Sci.*, 1996, **6**, 15–50.
27 G. Kresse and J. Hafner, *Phys. Rev. B: Condens. Matter Mater. Phys.*, 1993, **47**, 558–561.
28 G. Kresse and D. Joubert, *Phys. Rev. B: Condens. Matter Mater. Phys.*, 1999, **59**, 1758–1775.
29 K. B. Lejaeghere, G. Bihlmayer, T. Björkman, P. Blaha, S. Blügel, V. Blum, D. Caliste, I. E. Castelli, S. J. Clark, A. D. Corso, S. d. Gironcoli, T. Deutsch, J. K. Dewhurst, I. D. Marco, C. Draxl, M. Dułak, O. Eriksson, J. A. Flores-Livas, K. F. Garrity, L. Genovese, P. Giannozzi, M. Giantomassi, S. Goedecker, X. Gonze, O. Grånäs, E. K. U. Gross, A. Gulans, F. Gygi, D. R. Hamann, P. J. Hasnip, N. A. W. Holzwarth, D. Iuşan, D. B. Jochym, F. Jollet, D. Jones, G. Kresse, K. Koepernik, E. Küçükbenli, Y. O. Kvashnin, I. L. M. Locht, S. Lubeck, M. Marsman, N. Marzari, U. Nitzsche, L. Nordström, T. Ozaki, L. Paulatto, C. J. Pickard, W. Poelmans, M. I. J. Probert, K. Refson, M. Richter, G.-M. Rignanese, S. Saha, M. Scheffler, M. Schlipf, K. Schwarz, S. Sharma, F. Tavazza, P. Thunström, A. Tkatchenko, M. Torrent, D. Vanderbilt, M. J. v. Setten, V. V. Speybroeck, J. M. Wills, J. R. Yates, G.-X. Zhang and S. Cottenier, *Science*, 2016, **351**, aad3000.
30 J. Klimeš, D. R. Bowler and A. Michaelides, *Phys. Rev. B: Condens. Matter Mater. Phys.*, 2011, **83**, 195131.
31 J. Klimeš, D. R. Bowler and A. Michaelides, *J. Phys.: Condens. Matter*, 2010, **22**, 022201.
32 C. E. Umhey, J. Guo, Z. Cui, D. F. Shantz, A. Kulkarni and J.-S. McEwen, *Chem. Mater.*, 2024, **36**, 11852–11862.
33 A. Koishybay, C. Umhey, C. T. Kuo, K. Groden, J.-S. McEwen, A. M. Karim and D. F. Shantz, *ChemPhysChem*, 2023, **24**, e202300271.
34 R. Ransom, *Influence of the Synthesis Properties of Zeolite SSZ-39 on Composition and Catalytic Activity*, Tulane University School of Science and Engineering, 2019.
35 T. J. Boerner, S. Deems, T. R. Furlani, S. L. Knuth and J. Towns, *ACCESS: Advancing Innovation: NSF's Advanced Cyberinfrastructure Coordination Ecosystem: Services and Support*, Portland, OR, USA, 2023.